Front. Optoelectron. 2013, 6(2): 199–209
DOI 10.1007/s12200-013-0317-y

RESEARCH ARTICLE

SAGCM avalanche photodiode with additional layer and nonuniform electric field

Abbas GHADIMI (✉)[1], Vahid AHMADI (✉)[2], Fatemeh SHAHSHAHANI (✉)[3]

1 Department of Electrical Engineering, Science and Research Branch, Islamic Azad University, Tehran 145151775, Iran
2 Department of Electrical Engineering, Tarbiat Modares University, Tehran 14115-194, Iran
3 Department of Physics, Alzahra University, Tehran 1993893973, Iran

Abstract This paper presents a new method to increase the speed of the separated absorption, grading, charge, and multiplication avalanche photodiode (SAGCM-APD). This improvement is obtained by adding a new thin charge layer between absorption and grading layers, with assuming the non-uniform electric field in different regions of the structure. In addition, a circuit model of the proposed structure is extracted, using carrier rate equations. Also, to achieve the optimum structure, it is tried to have trade-offs among thickness of the layers and have proper tuning of physical parameters. Eventually, frequency and transient response are investigated and it is shown that, in comparison with the previous conventional structure, significant improvements in gain-bandwidth product, speed and also in breakdown voltage are attained.

Keywords separated absorption grading charge multiplication avalanche photodiode (SAGCM-APD), electric field nonuniformity, additional charge layer

1 Introduction

Avalanche photodiodes (APDs) are crucial components for long wavelength optical communication systems (OCS). In the past decade, the performance of APDs has been improved by amending the quality of applied materials and improvement of device structure [1]. In contrast to the positive-intrinsic-negative (PIN) photodiodes, APDs have an internal gain which causes higher detection sensitivity. For this reason, APD has become an efficient device with broad applications in long distance fiber OCS [2]. The gain-bandwidth product (GBP) is a key parameter. The large quantities of GBP enable APDs to work in high bit rates and provide them further future development. But, the randomness of the multiplication process produces excess noise and decreases device bandwidth. High performance APDs can be achieved by using separated absorption, grading, charge and multiplication (SAGCM) layers [3]. The APDs fabricated in this structure exhibit lower noise and higher bandwidth in comparison to other structures.

An equivalent circuit model was mostly used to evaluate the performance and to investigate the characteristics of an APD. Nowadays, several researches have been performed in order to model APDs [4–9]. But only a few of them have used SAGCM structure in their circuit modelings [10–15].

El-Batawy and Deen [10,11] introduced one of the earliest circuit models for SAGCM- APDs. But, the utilized transfer function for the gain computation of this model was difficult to be applied in opto-electronic integrated circuit (OEIC) software, and a uniform electric field was considered within the devices regions.

Uniformity assumption of the electric field in the multiplication region has a negative impact on modeling of real APDs [4,5]. Unfortunately, almost all presented models are based on uniform electric fields while the real electric field is not uniform.

Banoushi et al. [12] presented an alternative model for SAGCM-APDS that included dead space effect but ignored the non-uniformity of the electric field within the device regions. Wu and Wang [13,14] introduced circuit models of SAGCM-APD based on small signal and circuit elements. The models incorporated main bandwidth-limiting factors, such as carrier transit time, avalanche buildup time and external parasitic elements. But these two models also involved uniform electric field in the different regions of structures. Zhao and Mo [15] proposed an equivalent circuit model for resonant cavity enhanced-separated absorption grading charge multiplication avalanche photodiode (RCE-SAGCM-APD). They also conducted a detailed comparison among RCE-SAGCM-APDs

Received January 31, 2013; accepted February 19, 2013

E-mail: ghadimi555@yahoo.com, v_ahmadi@modares.ac.ir, f_shahshahani@alzahra.ac.ir

with different materials. But this model ignored the dead space effect and assumed uniformity of electric field in devices.

In this work, utilizing a basic high quality SAGCM structure, it is tried to improve its performance by adding a thin charge layer between absorption and grading layers in order to obtain a new structure. To properly model the device, the nonuniform electric field is assumed based on real inherent nonuniformity of the structure in different regions. Then a circuit model is extracted wherein, different aspects like, proper transfer function, dead space effect, carrier transit time, avalanche buildup time, external parasitic elements are considered. By simulating the model and analyzing different aspects influential on the device performance, it is tried to achieve the best widths of new charge layer and multiplication layer.

In the following sections, the details of the work are presented. The structure and the electric field profile, the carrier rate of different layers and extracted circuit model of the proposed SAGCM structure are presented in Sections 2, 3 and 4 respectively. Simulation results and comparisons with other conventional SAGCM structures are shown in Section 5 and the concluded remarks are presented in Section 6.

2 Structure and its electric field profile

A schematic structure of the APD under a typical illumination through p^+ side and its related electric field throughout the device are illustrated in Fig. 1. In this work, it is supposed that adding the new charge layer can cause an increase in primary transport speed of generating optical carriers from absorption layer (A) to multiplication layer (M) so that can improve the device performance compared to its predecessor. The new charge layer is referred to as (C_1) and the charge layer between grading and multiplication layer as (C_2).

In APDs, the primary carriers are produced by light absorption and then the secondary carriers are produced by the impact ionization effect. Both carriers contribute to the photocurrent. The electric field in absorption, first charge layer and grading regions are considered to be nonuniform. Second charge region and multiplication region are assumed to be fully depleted and the electric field of them is modeled by consecutive progressive steps. This assumption can simultaneously provide nonuniformity of the field, simplify the equation solution and make circuit model extraction easier. Impact ionization phenomena are considered to happen in multiplication and second charge layers due to their strong electric fields. The electric field profile, based on structural parameters and length of different layers can be described by following equations where q is the electron charge, ε is the permittivity and N_X is the doping concentration in X region, in which X can be M, A, C_1, G, C_2.

$$E_{\mathrm{p}}(x)=\frac{qN_{\mathrm{p}}}{\varepsilon_{\mathrm{p}}}(x+w_{\mathrm{p}}),\ -w_{\mathrm{p}}\leqslant x\leqslant 0, \tag{1}$$

$$E_{\mathrm{m}}(x)=\frac{qN_{\mathrm{p}}}{\varepsilon_{\mathrm{p}}}w_{\mathrm{p}}-\frac{qN_{\mathrm{m}}}{\varepsilon_{\mathrm{m}}}x,\ 0\leqslant x\leqslant w_{\mathrm{m}}, \tag{2}$$

$$E_{\mathrm{c}_2}(x)=\frac{qN_{\mathrm{p}}}{\varepsilon_{\mathrm{p}}}w_{\mathrm{p}}-\frac{qN_{\mathrm{m}}}{\varepsilon_{\mathrm{m}}}w_{\mathrm{m}}-\frac{qN_{\mathrm{c}_2}}{\varepsilon_{\mathrm{c}_2}}(x-w_{\mathrm{m}}),\quad w_{\mathrm{m}}\leqslant x\leqslant w_{\mathrm{m}}+w_{\mathrm{c}_2}, \tag{3}$$

$$E_{\mathrm{gr}}(x)=\frac{qN_{\mathrm{p}}}{\varepsilon_{\mathrm{p}}}w_{\mathrm{p}}-\frac{qN_{\mathrm{m}}}{\varepsilon_{\mathrm{m}}}w_{\mathrm{m}}-\frac{qN_{\mathrm{c}_2}}{\varepsilon_{\mathrm{c}_2}}w_{\mathrm{c}_2}-\frac{qN_{\mathrm{gr}}}{\varepsilon_{\mathrm{gr}}}(x-w_{\mathrm{m}}-w_{\mathrm{c}_2}),\quad w_{\mathrm{m}}+w_{\mathrm{c}_2}\leqslant x\leqslant w_{\mathrm{m}}+w_{\mathrm{c}_2}+w_{\mathrm{gr}}, \tag{4}$$

$$E_{\mathrm{c}_1}(x)=\frac{qN_{\mathrm{p}}}{\varepsilon_{\mathrm{p}}}w_{\mathrm{p}}-\frac{qN_{\mathrm{m}}}{\varepsilon_{\mathrm{m}}}w_{\mathrm{m}}-\frac{qN_{\mathrm{c}_2}}{\varepsilon_{\mathrm{c}_2}}w_{\mathrm{c}_2}-\frac{qN_{\mathrm{gr}}}{\varepsilon_{\mathrm{gr}}}w_{\mathrm{gr}}-\frac{qN_{\mathrm{c}_1}}{\varepsilon_{\mathrm{c}_1}}(x-w_{\mathrm{m}}-w_{\mathrm{c}_2}-w_{\mathrm{gr}}),\quad w_{\mathrm{m}}+w_{\mathrm{c}_2}+w_{\mathrm{gr}}\leqslant x\leqslant w_{\mathrm{m}}+w_{\mathrm{c}_2}+w_{\mathrm{gr}}+w_{\mathrm{c}_1}, \tag{5}$$

$$E_{\mathrm{a}}(x)=\frac{qN_{\mathrm{p}}}{\varepsilon_{\mathrm{p}}}w_{\mathrm{p}}-\frac{qN_{\mathrm{m}}}{\varepsilon_{\mathrm{m}}}w_{\mathrm{m}}-\frac{qN_{\mathrm{c}_2}}{\varepsilon_{\mathrm{c}_2}}w_{\mathrm{c}_2}-\frac{qN_{\mathrm{gr}}}{\varepsilon_{\mathrm{gr}}}w_{\mathrm{gr}}-\frac{qN_{\mathrm{c}_1}}{\varepsilon_{\mathrm{c}_1}}w_{\mathrm{c}_1}-\frac{qN_{\mathrm{a}}}{\varepsilon_{\mathrm{a}}}(x-w_{\mathrm{m}}-w_{\mathrm{c}_2}-w_{\mathrm{gr}}-w_{\mathrm{c}_1}),\quad w_{\mathrm{m}}+w_{\mathrm{c}_2}+w_{\mathrm{gr}}+w_{\mathrm{c}_1}\leqslant x\leqslant w_{\mathrm{m}}+w_{\mathrm{c}_2}+w_{\mathrm{gr}}+w_{\mathrm{c}_1}+w_{\mathrm{a}}, \tag{6}$$

$$E_{\mathrm{n}}(x)=\frac{qN_{\mathrm{p}}}{\varepsilon_{\mathrm{p}}}w_{\mathrm{p}}-\frac{qN_{\mathrm{m}}}{\varepsilon_{\mathrm{m}}}w_{\mathrm{m}}-\frac{qN_{\mathrm{c}_2}}{\varepsilon_{\mathrm{c}_2}}w_{\mathrm{c}_2}-\frac{qN_{\mathrm{gr}}}{\varepsilon_{\mathrm{gr}}}w_{\mathrm{gr}}-\frac{qN_{\mathrm{c}_1}}{\varepsilon_{\mathrm{c}_1}}w_{\mathrm{c}_1}-\frac{qN_{\mathrm{a}}}{\varepsilon_{\mathrm{a}}}w_{\mathrm{a}}-\frac{qN_{\mathrm{n}}}{\varepsilon_{\mathrm{n}}}(x-w_{\mathrm{m}}-w_{\mathrm{c}_2}-w_{\mathrm{gr}}-w_{\mathrm{c}_1}-w_{\mathrm{a}}),\quad w_{\mathrm{m}}+w_{\mathrm{c}_2}+w_{\mathrm{gr}}+w_{\mathrm{c}_1}+w_{\mathrm{a}}\leqslant x\leqslant w_{\mathrm{m}}+w_{\mathrm{c}_2}+w_{\mathrm{gr}}+w_{\mathrm{c}_1}+w_{\mathrm{a}}+w_{\mathrm{n}}. \tag{7}$$

To consider the spatial dependence of the electric field in an equivalent circuit model, a staircase approximate model, as shown in Fig. 2, can be beneficial. The electric field in multiplication region and the second charge region are modeled by consecutive progressive steps. To proceed, one needs to know the exact profile of the electric field in all regions. The electric field profile in the second charge region and multiplication region are supposed to be divided into four constant sections with equal steps.

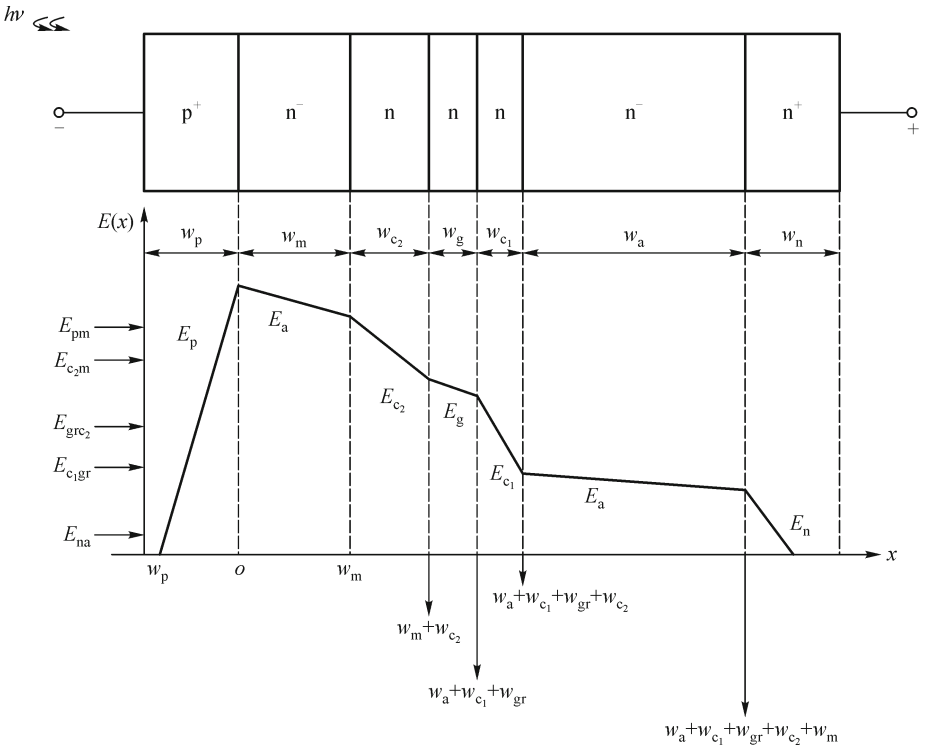

Fig. 1 Schematic structure and electric field profile of APD

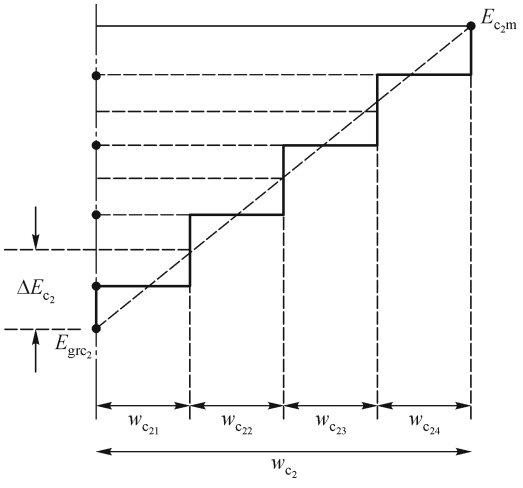

Fig. 2 Electric field division with staircase approximation model

3 Carrier rate equations

For developing a circuit model, we must deduce the carrier rate equations in the different regions. These equations for this approximate model in various regions are

p^+ region :

$$\frac{\mathrm{d}n_\mathrm{p}}{\mathrm{d}t} = N_\mathrm{Gp} - \frac{n_\mathrm{p}}{\tau_\mathrm{nrp}} - \frac{In}{q} \ \& \ N_\mathrm{Gp} \approx 0, \tag{8}$$

n^-(A region) :

$$\frac{\mathrm{d}p_\mathrm{a}}{\mathrm{d}t} = P_\mathrm{Ga} - \frac{p_\mathrm{a}}{\tau_\mathrm{pra}} - \frac{p_\mathrm{a}}{\tau_\mathrm{pta}} + \frac{In}{q}, \tag{9}$$

n (C_1 region) :

$$\frac{\mathrm{d}p_{c_1}}{\mathrm{d}t} = P_{\mathrm{Gc}_1} - \frac{p_{c_1}}{\tau_{\mathrm{prc}_1}} - \frac{p_{c_1}}{\tau_{\mathrm{ptc}_1}}, \tag{10}$$

n (G region) :

$$\frac{\mathrm{d}p_\mathrm{g}}{\mathrm{d}t} = P_\mathrm{Ggr} - \frac{p_\mathrm{gr}}{\tau_\mathrm{prgr}} - \frac{p_\mathrm{gr}}{\tau_\mathrm{ptgr}}, \tag{11}$$

n (C_2 region) :

$$\begin{cases} \dfrac{\mathrm{d}P_{c_{21}}}{\mathrm{d}t} = P_{\mathrm{Gc}_{21}} + (\alpha_{c_{21}}\nu_{\mathrm{nc}_{21}} + \beta_{c_{21}}\nu_{\mathrm{pc}_{21}})P_{c_{21}} - \dfrac{P_{c_{21}}}{\tau_{\mathrm{prc}_{21}}} - \dfrac{P_{c_{21}}}{\tau_{\mathrm{ptc}_{21}}}, \\ \dfrac{\mathrm{d}P_{c_{22}}}{\mathrm{d}t} = P_{\mathrm{Gc}_{22}} + (\alpha_{c_{22}}\nu_{\mathrm{nc}_{22}} + \beta_{c_{22}}\nu_{\mathrm{pc}_{22}})P_{c_{22}} - \dfrac{P_{c_{22}}}{\tau_{\mathrm{prc}_{22}}} - \dfrac{P_{c_{22}}}{\tau_{\mathrm{ptc}_{22}}}, \\ \dfrac{\mathrm{d}P_{c_{23}}}{\mathrm{d}t} = P_{\mathrm{Gc}_{23}} + (\alpha_{c_{23}}\nu_{\mathrm{nc}_{23}} + \beta_{c_{23}}\nu_{\mathrm{pc}_{23}})P_{c_{23}} - \dfrac{P_{c_{23}}}{\tau_{\mathrm{prc}_{23}}} - \dfrac{P_{c_{23}}}{\tau_{\mathrm{ptc}_{23}}}, \\ \dfrac{\mathrm{d}P_{c_{24}}}{\mathrm{d}t} = P_{\mathrm{Gc}_{24}} + (\alpha_{c_{24}}\nu_{\mathrm{nc}_{24}} + \beta_{c_{24}}\nu_{\mathrm{pc}_{24}})P_{c_{24}} - \dfrac{P_{c_{24}}}{\tau_{\mathrm{prc}_{24}}} - \dfrac{P_{c_{24}}}{\tau_{\mathrm{ptc}_{24}}}, \end{cases} \tag{12}$$

n (M region) :

$$\begin{cases} \dfrac{\mathrm{d}P_{\mathrm{m}_1}}{\mathrm{d}t} = P_{\mathrm{Gm}_1} + (\alpha_{\mathrm{m}_1}\nu_{\mathrm{nm}_1} + \beta_{\mathrm{m}_1}\nu_{\mathrm{pm}_1})P_{\mathrm{m}_1} \\ \qquad -\dfrac{P_{\mathrm{m}_1}}{\tau_{\mathrm{prm}_1}} - \dfrac{P_{\mathrm{m}_1}}{\tau_{\mathrm{ptm}_1}} + \dfrac{I_{p_1}}{q}, \\ \dfrac{\mathrm{d}P_{\mathrm{m}_2}}{\mathrm{d}t} = P_{\mathrm{Gm}_2} + (\alpha_{\mathrm{m}_2}\nu_{\mathrm{nm}_2} + \beta_{\mathrm{m}_2}\nu_{\mathrm{pm}_2})P_{\mathrm{m}_2} \\ \qquad -\dfrac{P_{\mathrm{m}_2}}{\tau_{\mathrm{prm}_2}} - \dfrac{P_{\mathrm{m}_2}}{\tau_{\mathrm{ptm}_2}} + \dfrac{I_{\mathrm{p}_2}}{q}, \\ \dfrac{\mathrm{d}P_{\mathrm{m}_3}}{\mathrm{d}t} = P_{\mathrm{Gm}_3} + (\alpha_{\mathrm{m}_3}\nu_{\mathrm{nm}_3} + \beta_{\mathrm{m}_3}\nu_{\mathrm{pm}_3})P_{\mathrm{m}_3} \\ \qquad -\dfrac{P_{\mathrm{m}_3}}{\tau_{\mathrm{prm}_3}} - \dfrac{P_{\mathrm{m}_3}}{\tau_{\mathrm{ptm}_3}} + \dfrac{I_{\mathrm{p}_3}}{q}, \\ \dfrac{\mathrm{d}P_{\mathrm{m}_4}}{\mathrm{d}t} = P_{\mathrm{Gm}_4} + (\alpha_{\mathrm{m}_4}\nu_{\mathrm{nm}_4} + \beta_{\mathrm{m}_4}\nu_{\mathrm{pm}_4})P_{\mathrm{m}_4} \\ \qquad -\dfrac{P_{\mathrm{m}_4}}{\tau_{\mathrm{prm}_4}} - \dfrac{P_{\mathrm{m}_4}}{\tau_{\mathrm{ptm}_4}} + \dfrac{I_{\mathrm{p}_4}}{q}, \end{cases} \tag{13}$$

n^+region :

$$\frac{\mathrm{d}P_{\mathrm{n}}}{\mathrm{d}t} = P_{\mathrm{Gn}} - \frac{P_{\mathrm{n}}}{\tau_{\mathrm{prn}}} - \frac{I_{\mathrm{p}}}{q} \;\&\; P_{\mathrm{Gn}} \approx 0, \tag{14}$$

where $(n_{\mathrm{p}},\tau_{\mathrm{nrp}})$ and $(p_{\mathrm{n}},\tau_{\mathrm{prn}})$ are the total numbers of excess minority carriers and recombination lifetimes in the p^+ and n^+ regions, and $\left(p_{\mathrm{m(a,c_1,g,c_2)}},\tau_{\mathrm{prm(a,c_1,g,c_2)}},\tau_{\mathrm{ptm(a,c_1,g,c_2)}}\right)$ are the total numbers of holes and their corresponding recombination lifetimes and transit time in M or A or C_1 or G or C_2 region respectively. Rates of the electron–hole pair photo-generation in these regions are shown by $N_{\mathrm{Gp}},P_{\mathrm{Ga}},P_{\mathrm{Gc_1}},P_{\mathrm{Ggr}},P_{\mathrm{Gc_2}},P_{\mathrm{Gm}},P_{\mathrm{Gn}}$. Also, I_{n}, I_{p} are the minority electron and hole currents in p^+ and n^+ regions, $(v_{\mathrm{nm}},v_{\mathrm{pm}})$ and $(v_{\mathrm{nc_2}},v_{\mathrm{pc_2}})$ are the electron and hole drift velocities in the M and C_2 regions respectively. The dependence of the carrier drift velocities into field is given in Ref. [9]. α and β are the electron and hole impact ionization rates, respectively. To take the effects of dead spaces for carriers in our circuit modeling, the simple method introduced in Ref. [7] is used. The dead space of carriers is defined as below, where $E_{\mathrm{th;e(h)}}$ indicates the ionization threshold energy of the electron (hole).

The first formula for dead space is

$$d_{\mathrm{e,h}} = \frac{E_{\mathrm{th;e,h}}}{qF}. \tag{15}$$

But by considering E_0 (initial energy before starting dead space), the dead space formulas are

$$d_{\mathrm{e,h}} = \frac{E_{\mathrm{th;e,h}} - E_0}{qF}, \tag{16}$$

$$\alpha(x) = \alpha(F)u(x - d_{\mathrm{e}}), \tag{17}$$

$$\beta(x) = \beta(F)u(x - d_{\mathrm{h}}). \tag{18}$$

E_{th} of electron and hole are defined as below, where E_0 is the initial energy of the carrier.

$$E_{\mathrm{th;e}} - E_0 = \int_0^{d_{\mathrm{e}}} F(x)\mathrm{d}x, \tag{19}$$

$$E_{\mathrm{th;h}} - E_0 = \int_{W_{\mathrm{m}} - d_{\mathrm{h}}}^{d_{\mathrm{h}}} F(x)\mathrm{d}x. \tag{20}$$

The electron and hole ionization coefficients are defined as below [16–19];

$$\alpha(F) = a_{\mathrm{n}}\exp\left(-\frac{b_{\mathrm{n}}}{F}\right)^{c_{\mathrm{n}}}, \tag{21}$$

$$\beta(F) = a_{\mathrm{p}}\exp\left(-\frac{b_{\mathrm{p}}}{F}\right)^{c_{\mathrm{p}}}, \tag{22}$$

where a_{n} and a_{p}, b_{n} and b_{p}, c_{n} and c_{p} are the constant parameters of material.

4 Circuit model

To achieve an equivalent circuit model for the device, first, the physical quantities should be converted to the corresponding circuit quantities. In this regard, a constant capacitor value, C_0, is used to convert the charge into corresponding voltage. By dividing the carrier charge of each region into C_0, the equivalent voltage of the carriers in each region can be obtained [13]. The equivalent resistors of each region can be calculated by considering the different voltages, the carrier's combination process and also the photo generation rate in the different regions. The resistor values can be obtained from Eqs. (34) to (38). Obtained circuit model of this structure is shown in Fig. 3.

The current components shown in Fig. 3 can be written as below:

$$I_{\mathrm{n}} = \frac{V_1}{R_{\mathrm{nd}}} + I_{n_{\mathrm{o}}} + \beta_{\mathrm{n}}P_{\mathrm{in}}, \tag{23}$$

$$I_{\mathrm{op}} = qN_{\mathrm{Gp}} = \frac{P_{\mathrm{in}}}{R_1} = C_{P_{\mathrm{o}}}\frac{\mathrm{d}V_1}{\mathrm{d}t} + \frac{V_1}{R_{\mathrm{n}}} + I_{\mathrm{n}}, \tag{24}$$

$$I_{o_{\mathrm{a}}} = qp_{\mathrm{Ga}} = \frac{P_{\mathrm{in}}}{R_2} = C_{a_{\mathrm{o}}}\frac{\mathrm{d}V_2}{\mathrm{d}t} + \frac{V_2}{R_{\mathrm{a}}} + \frac{V_2}{R_{\mathrm{ta}}} - I_{\mathrm{n}}, \tag{25}$$

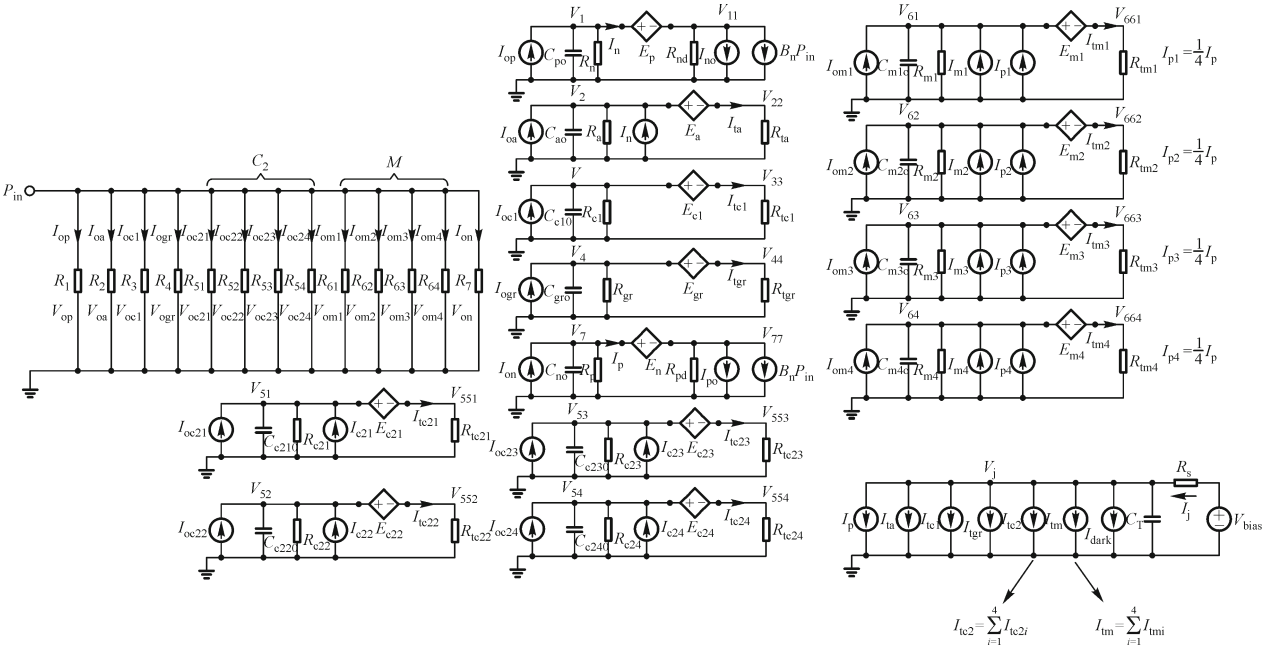

Fig. 3 Circuit model of proposed structure

$$I_{o_{c_1}} = qp_{Gc_1} = \frac{P_{in}}{R_3} = C_{c_{10}}\frac{dV_3}{dt} + \frac{V_3}{R_{c1}} + \frac{V_3}{R_{tc1}}, \tag{26}$$

$$I_{o_{gr}} = qp_{Ggr} = \frac{P_{in}}{R_4} = C_{gr_0}\frac{dV_4}{dt} + \frac{V_4}{R_{gr}} + \frac{V_4}{R_{tgr}}, \tag{27}$$

$$\begin{aligned} I_{o_{c_{2i}}} &= qp_{Gc_{2i}} = \frac{P_{in}}{R_{5i}} \\ &= C_{c_{210}}\frac{dV_{5i}}{dt} - (\alpha_{c_{2i}}\nu_{nc_{2i}} + \beta_{c_{2i}}\nu_{pc_{2i}})C_{c_{210}}V_{5i} \\ &\quad + \frac{V_{5i}}{R_{c2i}} + \frac{V_{5i}}{R_{tc2i}},\ 1\langle i\langle 4, \end{aligned} \tag{28}$$

$$I_{C_{2i}} = (\alpha_{c_{2i}}\nu_{nc_{2i}} + \beta_{c_{2i}}\nu_{pc_{2i}})C_{c_{2i0}}V_{5i}, \tag{29}$$

$$\begin{aligned} I_{o_{mi}} &= qp_{Gmi} = \frac{P_{in}}{R_{6i}} \\ &= C_{m_{10}}\frac{dV_{6i}}{dt} - (\alpha_{mi}\nu_{nmi} + \beta_{mi}\nu_{pmi})C_{m_{10}}V_{6i} \\ &\quad + \frac{V_{6i}}{R_{mi}} + \frac{V_{6i}}{R_{tmi}} - I_{p_1},\ 1\langle i\langle 4, \end{aligned} \tag{30}$$

$$I_{mi} = (\alpha_{mi}\nu_{nmi} + \beta_{mi}\nu_{pmi})C_{m_{10}}V_{6i}, \tag{31}$$

$$I_{p_o} = \frac{qp_{n_o}L_p\left(\cosh\left(\frac{W_n}{L_p}\right) + 1\right)}{W_n\tau_{prn}\sinh\left(\frac{W_n}{L_p}\right)}, \tag{32}$$

$$P_{n_0} = p_{n_0}Aw_n = \frac{n_n^2}{N_d}AW_n,$$

$$I_{n_o} = \frac{qN_{p_o}L_n\left(\cosh\left(\frac{W_p}{L_n}\right) + 1\right)}{W_p\tau_{rnp}\sinh\left(\frac{W_p}{L_n}\right)}, \tag{33}$$

$$N_{P_0} = n_{p_0}w_pA = \frac{n_p^2}{N_a}AW_p,$$

where

$$R_{m_i} = \frac{\tau_{prmi}}{C_{m_{i0}}},\ R_{tmi} = \frac{\tau_{ptmi}}{C_{m_{i0}}},\ R_n = \frac{\tau_{rnp}}{C_{p_0}},\ R_a = \frac{\tau_{pra}}{C_{a_o}},\ R_{gr} = \frac{\tau_{prgr}}{C_{gr_0}},\ 1\langle i\langle 4, \tag{34}$$

$$R_{c_1} = \frac{\tau_{prc_1}}{C_{c_{10}}},\ R_{tc_1} = \frac{\tau_{ptc_1}}{C_{c_{10}}},\ R_{ta} = \frac{\tau_{pta}}{C_{a_o}},\ R_{tgr} = \frac{\tau_{ptgr}}{C_{gr_0}}, \tag{35}$$

$$R_{c_{2i}} = \frac{\tau_{prc_{2i}}}{C_{c_{2i0}}},\ R_{tc_{2i}} = \frac{\tau_{ptc_{2i}}}{C_{c_{2i0}}},\ 1\langle i\langle 4, \tag{36}$$

$$R_{\rm pd} = R_{\rm p}\left(\cosh\left(\frac{W_{\rm p}}{L_{\rm p}}\right)-1\right),\ L_{\rm p} = \sqrt{D_{\rm p}\tau_{\rm prn}}, \quad (37)$$

$$R_{\rm nd} = R_{\rm n}\left(\cosh\left(\frac{W_{\rm p}}{L_{\rm n}}\right)-1\right),\ L_{\rm n} = \sqrt{D_{\rm n}\tau_{\rm rnp}}. \quad (38)$$

Photo-generation rates are defined as below:

$$N_{\rm Gp} = \frac{P_{\rm in}(1-R)}{h\nu}(1-{\rm e}^{-\alpha_{\rm p}w_{\rm p}}), \quad (39)$$

$$P_{\rm Ga} = \frac{P_{\rm in}(1-R)}{h\nu}{\rm e}^{-\alpha_{\rm p}w_{\rm p}}(1-{\rm e}^{-\alpha_{\rm a}w_{\rm a}}), \quad (40)$$

$$P_{\rm Gc_1} = \frac{P_{\rm in}(1-R)}{h\nu}{\rm e}^{-\alpha_{\rm p}w_{\rm p}-\alpha_{\rm a}w_{\rm a}}(1-{\rm e}^{-\alpha_{\rm c_1}w_{\rm c_1}}), \quad (41)$$

$$P_{\rm Ggr} = \frac{P_{\rm Gc_1}}{(1-{\rm e}^{-\alpha_{\rm c_1}w_{\rm c_1}})}{\rm e}^{-\alpha_{\rm c_1}w_{\rm c_1}}(1-{\rm e}^{-\alpha_{\rm gr}w_{\rm gr}}), \quad (42)$$

$$P_{\rm Gc21} = \frac{P_{\rm Ggr}}{(1-{\rm e}^{-\alpha_{\rm gr}w_{\rm gr}})}{\rm e}^{-\alpha_{\rm gr}w_{\rm gr}}(1-{\rm e}^{-\alpha_{\rm c21}w_{\rm c21}}), \quad (43)$$

$$P_{\rm Gc22} = \frac{P_{\rm Gc21}}{(1-{\rm e}^{-\alpha_{\rm c21}w_{\rm c21}})}{\rm e}^{-\alpha_{\rm c21}w_{\rm c21}}(1-{\rm e}^{-\alpha_{\rm c22}w_{\rm c22}}), \quad (44)$$

$$P_{\rm Gc23} = \frac{P_{\rm Gc22}}{(1-{\rm e}^{-\alpha_{\rm c22}w_{\rm c22}})}{\rm e}^{-\alpha_{\rm c22}w_{\rm c22}}(1-{\rm e}^{-\alpha_{\rm c23}w_{\rm c23}}), \quad (45)$$

$$P_{\rm Gc24} = \frac{P_{\rm Gc23}}{(1-{\rm e}^{-\alpha_{\rm c23}w_{\rm c23}})}{\rm e}^{-\alpha_{\rm c23}w_{\rm c23}}(1-{\rm e}^{-\alpha_{\rm c24}w_{\rm c24}}), \quad (46)$$

$$P_{\rm Gm1} = \frac{P_{\rm Gc24}}{(1-{\rm e}^{-\alpha_{\rm c24}w_{\rm c24}})}{\rm e}^{-\alpha_{\rm c24}w_{\rm c24}}(1-{\rm e}^{-\alpha_{\rm Gm1}w_{\rm Gm1}}), \quad (47)$$

$$P_{\rm Gm2} = \frac{P_{\rm Gm1}}{(1-{\rm e}^{-\alpha_{\rm Gm1}w_{\rm Gm1}})}{\rm e}^{-\alpha_{\rm Gm1}w_{\rm Gm1}}(1-{\rm e}^{-\alpha_{\rm Gm2}w_{\rm Gm2}}), \quad (48)$$

$$P_{\rm Gm3} = \frac{P_{\rm Gm2}}{(1-{\rm e}^{-\alpha_{\rm Gm2}w_{\rm Gm2}})}{\rm e}^{-\alpha_{\rm Gm2}w_{\rm Gm2}}(1-{\rm e}^{-\alpha_{\rm Gm3}w_{\rm Gm3}}), \quad (49)$$

$$P_{\rm Gm4} = \frac{P_{\rm Gm3}}{(1-{\rm e}^{-\alpha_{\rm Gm3}w_{\rm Gm3}})}{\rm e}^{-\alpha_{\rm Gm3}w_{\rm Gm3}}(1-{\rm e}^{-\alpha_{\rm Gm4}w_{\rm Gm4}}), \quad (50)$$

$$P_{\rm n} = \frac{P_{\rm Gm4}}{(1-{\rm e}^{-\alpha_{\rm Gm4}w_{\rm Gm4}})}{\rm e}^{-\alpha_{\rm Gm4}w_{\rm Gm4}}(1-{\rm e}^{-\alpha_{\rm n}w_{\rm n}}), \quad (51)$$

where $P_{\rm in}$ is the optical power, R is the reflectivity, and $h\nu$ is the photon energy. α_X is the absorption coefficient and W_X is the width of the X (M or A or C_1 or G or C_2) region.

5 Simulation result, comparison and discussion

To verify the accuracy of the model, the InP/InGaAs APD of Ref. [12] has been improved by additional charge layer and then the results of the proposed model have been compared with its conventional predecessor. The parameters for simulation have been taken from Refs. [20–22] and some of them listed in Table 1.

To examine the response speed of the device, some simulations have been performed. The response to a Gaussian pulse with 10 ps width and 100 μW power is shown in Fig. 4. This curve is compared with different probability functions, such as Lognormal, Rayleigh, Maxwell, Gamma (Erlang). Finally, it was found that, the curve has been mostly compatible with the Lognormal probability distribution function. The property of Lognormal function has been employed to reach the highest peak with the lowest rising time. Fulfilling this criterion, has given us the optimum value for $w_{\rm c_1}$ = 39.8 nm.

In this figure, a comparison between the proposed structure time response with different new charge layer widths and the conventional one with $w_{\rm c_1}$ = 0 has been drawn. It is shown that the rising time will decrease with the growth of $w_{\rm c_1}$ until a certain value, where afterwards the trend is inverse. As it can be easily seen, the device performance has improved due to additional layer and the

Table 1 Some parameters of APD

parameter	value	parameter	value
$N_{\rm n}$/cm^{-3}	1.5×10^{17}	$a_{\rm p}$	2.1×10^{6}
$N_{\rm m}$/cm^{-3}	7×10^{14}	$b_{\rm p}$	1.77
$N_{\rm p}$/cm^{-3}	1×10^{18}	$c_{\rm p}$	1.15
$W_{\rm n}$/nm	50	$E_{\rm thp}$/eV	3
$W_{\rm m}$/nm	200	$E_{\rm the}$/eV	2.8
$W_{\rm p}$/nm	50	$v_{\rm sp}$/(cm·s^{-1})	0.33×10^{7}
$\alpha_{\rm n}$/cm^{-1}	3.5×10^{4}	$v_{\rm sn}$/(cm·s^{-1})	0.67×10^{7}
$\alpha_{\rm m}$/cm^{-1}	1×10^{4}	$C_{\rm s}$/pF	0.31
$\alpha_{\rm p}$/cm^{-1}	3.5×10^{4}	$R_{\rm s}$/Ω	20

best performance has been achieved in 39.8 nm thickness.

In addition to the effect of w_{c_1} on rise time decreasing, Fig. 4 shows that, the output current has the largest amplitude in optimum value of w_{c_1}. By increasing the width of the C_1 layer up to 39.8 nm, gain increases and afterwards has a falling trend.

Figure 5 shows the detector response to step pulse with 1 μW input power in various thickness of the C_1 layer in order to examine the device slew rate. In fact, slew rate is the ratio of output changes to the time changes and mainly obtained from step response of the device.

Figure 6 is an inset of the curves in the zoomed region of Fig. 5. The zoomed region depicts 14 percent of the slew rate increment at the optimum thickness comparing to conventional SAGCM.

It can be seen in Fig. 6 that, the thicker C_1 layer is, the more output current we have, which means higher gain. Also in higher widths of added layer, the output current has

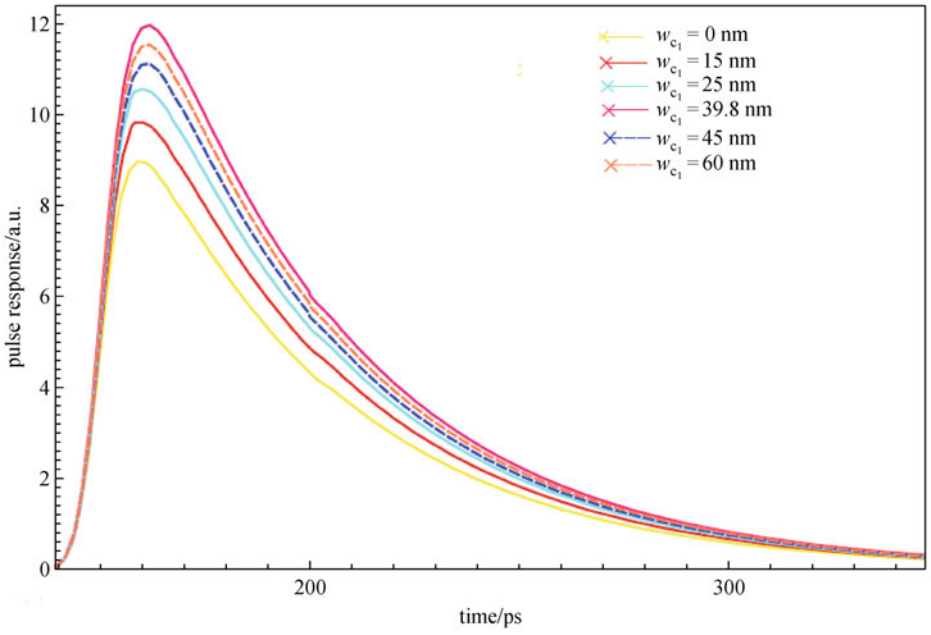

Fig. 4 Gaussian pulse response in various thicknesses of w_{c_1} (w_m = 200 nm, w_{c_2} = 60 nm)

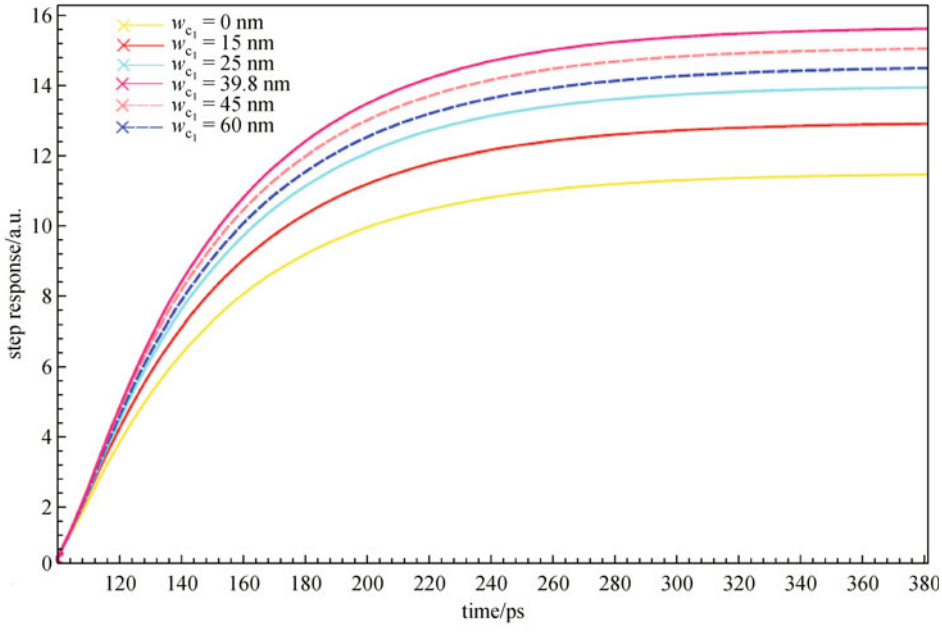

Fig. 5 Step pulse response for various charge layer thicknesses (w_m = 200 nm, w_{c_2} = 60 nm)

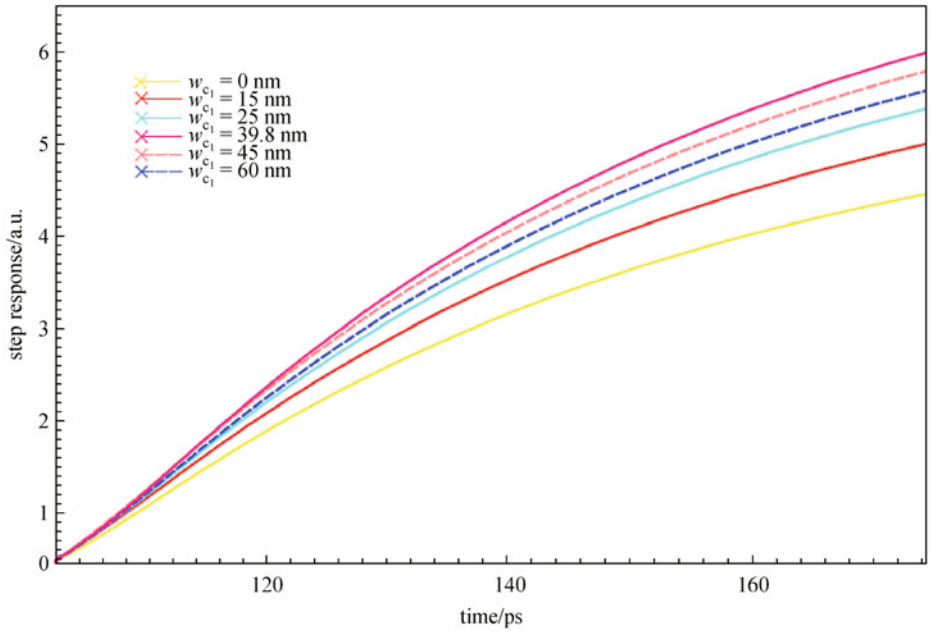

Fig. 6 Inset of the curves in the zoomed region of Fig. 5

faster response due to more photo carrier's generation in a specific time span that can be explained by slew rate. It should mention that the same optimum value is repeated here because after this value, slew rate decreases.

To show the effect of the new charge layer on the gain-bandwidth characteristics of the proposed structure, the device is simulated in different first charge layer widths (w_{c_1}) from 0 to 60 nm, in constant thickness of 200 nm for multiplication layer and 60 nm for the second charge layer. The result is plotted in Fig. 7, which illustrates the maximum gain-bandwidth product occurs in w_{c_1} = 39.8 nm with a growth of about 11% in comparison with w_{c_1} = 0 nm.

In fact, the control of the layer thickness, which in turn would result in corresponding changes in electric field, can lead to this result. It is obvious that the higher thickness can

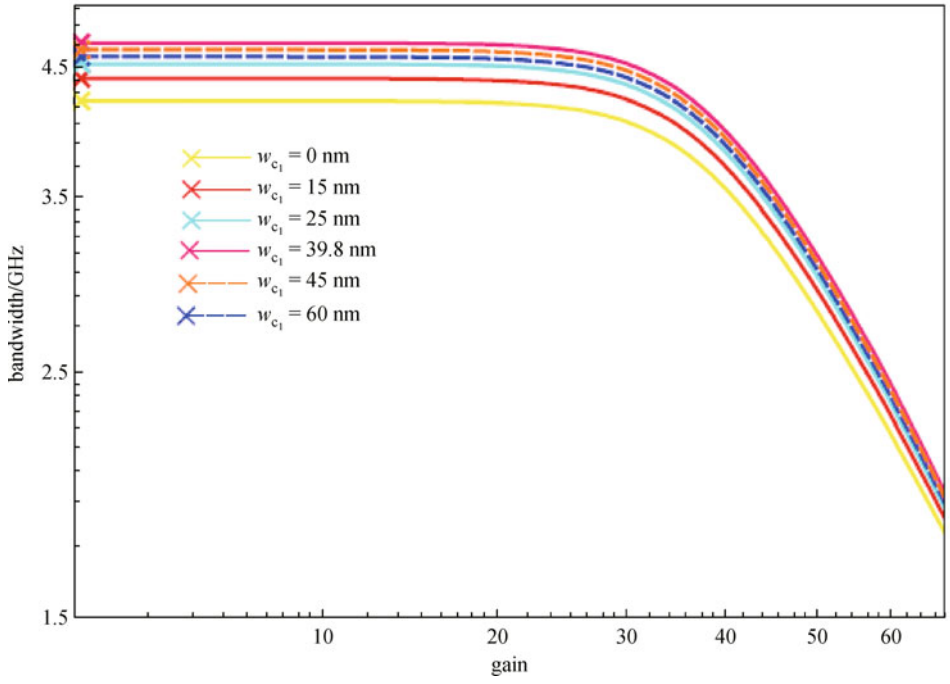

Fig. 7 Bandwidth versus gain in various thicknesses of w_{c_1} (w_m = 200 nm, w_{c_2} = 60 nm)

increase transit time and the higher electric field can accelerate the carrier. Accordingly, there is interaction between thickness and electric field. This interaction for thicknesses up to 39.8 nm is in a way that GBP has upwards trend and afterwards the trend is downwards.

Since, the role of the additional charge layer has been proven in the improvement of the bandwidth characteristics of the APD, a natural question comes to mind; whether this proposed structure can exhibit an improvement in breakdown characteristic or not.

As multiplication is the cause of breakdown phenomenon, the effect of the M layer has been investigated in breakdown voltage performance. The results are presented in Fig. 8. It can be easily inferred that the breakdown voltage is in direct proportion with multiplication layer thickness.

To investigate the effect of w_{c_1} presence and its changes on breakdown voltage, some simulations have been done that is presented in Fig. 9. In this regard, to the SAGCM with 400 nm multiplication layer thickness that is intro-

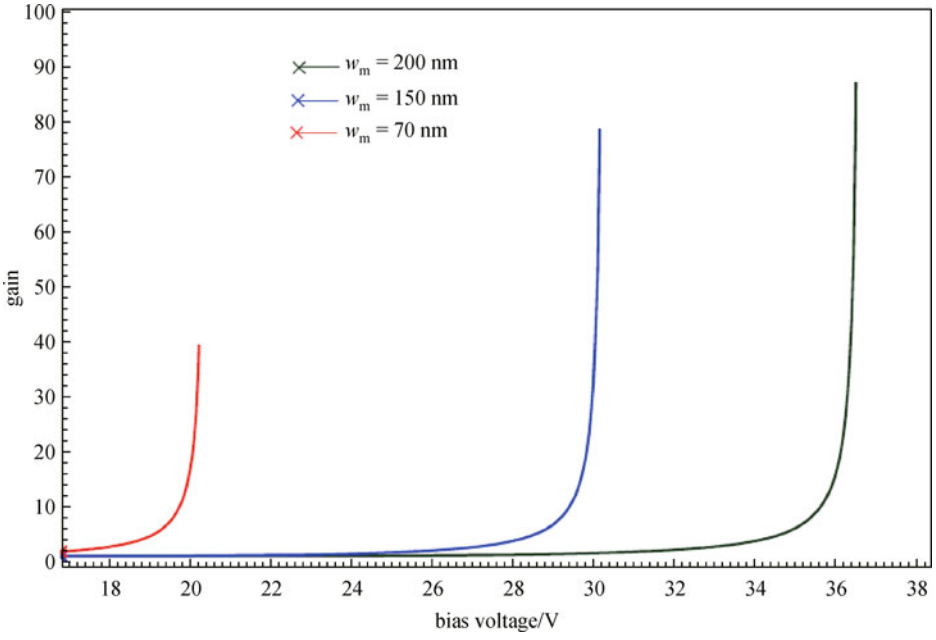

Fig. 8 Breakdown voltage based on different widths of multiplication layer

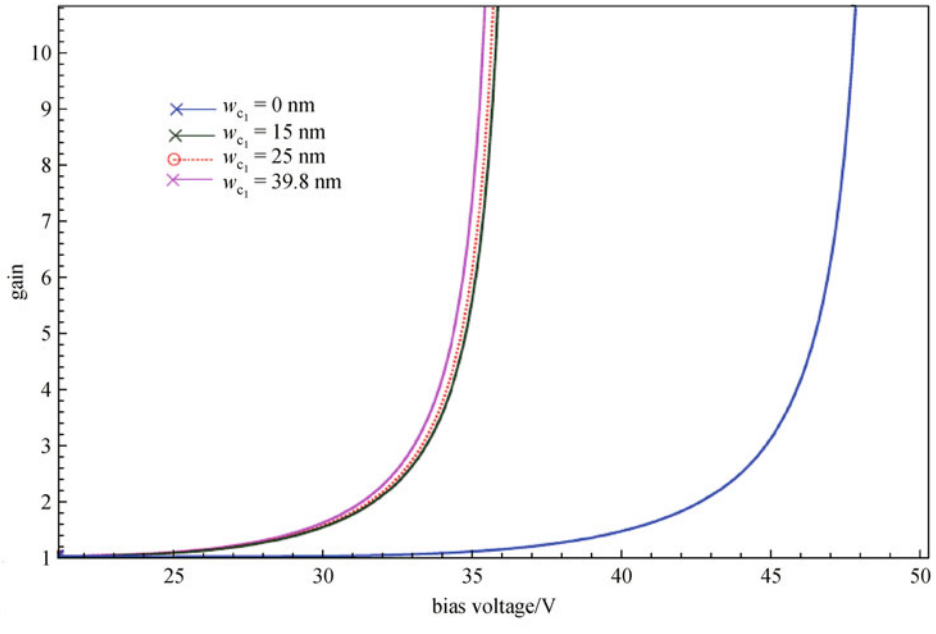

Fig. 9 Changes of breakdown voltage in different thicknesses of C_1 charge layer

duced in Ref. [12] with a breakdown voltage of about 48.3 V, a C_1 layer with thickness of 39.8 nm has been added and a significant improvement achieved.

The breakdown voltage has been around 36.3 V in comparison with 48.3 V. It also shows that by changing the width of C_1 from 5 to 39.8 nm, the breakdown voltage has remained clearly unchanged. As a result, it can be said that the presence of first charge layer is very important to improve breakdown voltage but its variation has negligible effect on its value.

Finally, all the presented results show that the simulation of optimized proposed structure has provided better performance in comparison with the conventional SAGCM.

6 Conclusions

In this paper, the advantages of adding a thin charge layer in a non-uniform electric field SAGCM-APD structure has been investigated in order to achieve a high performance structure. Also, using carrier rate equations, a circuit model has been extracted. Then, the effects of additional layer on transient criterion, such as slew-rate, rising and falling times, have been examined. It has been shown that the time response curve is more compatible with the Lognormal probability distribution function. To achieve optimum values of the layer thicknesses, that are influential on band width, GBP and breakdown voltage of the proposed structure, some tradeoffs have been done based on performed simulations. In this regard, it has been shown that controlling the widths of new additional layer beside multiplication layer can cause a significant improvement in breakdown voltage and GBP. Finally, all results show that the proposed structure exhibits a superior performance in comparison with the other conventional SAGCMs.

References

1. Campbell J C. Recent advances in telecommunications avalanche photodiodes. Journal of Lightwave Technology, 2007, 25(1): 109–121
2. Kasper B L, Campbell J C. Multigigbit-per-second avalanche photodiode lightwave receivers. Journal of Lightwave Technology, 1987, 5(10): 1351–1364
3. Tarof L E, Yu J, Bruce R, Knight D G, Baird T, Oosterbrink B. High-frequency performance of separate absorption and multiplication InP/InGaAs avalanche photodiodes. IEEE Photonics Technology Letters, 1993, 5(6): 672–674
4. Masudy-Panah S, Moravvej-Farshi M K, Jalali M. Temperature dependent characteristics of submicron GaAs avalanche photodiodes obtained by a nonlocal analysis. Journal of Optical Communications and Networking, 2009, 282(17): 3630–3636
5. Liew S C, Tan C H, Goh Y L, Marshall A R J, David J P R. Modeling of avalanche multiplication and excess noise factor in $In_{0.52}Al_{0.48}As$ avalanche photodiodes using a simple Monte Carlo model. Journal of Applied Physics, 2008, 104(19): 13114–13119
6. Banoushi A, Ahmadi V, Setayeshi S. An analytical approach to study the effect of carrier velocities on the gain and breakdown voltage of avalanche photodiodes. Journal of Lightwave Technology, 2002, 20(4): 696–699
7. Ng B K, David J P R, Plimmer S A, Rees G J, Tozer R C, Hopkinson M, Hill G. Avalanche multiplication characteristics of $Al_{0.8}$ $Ga_{0.2}$ As diodes. IEEE Transactions on Electron Devices, 2001, 48(10): 2198–2204
8. Bandyopadhyay A, Deen M J, Tarof L E, Clark W A. Simplified approaches to time-domain modeling of avalanche photodiodes. IEEE Journal of Quantum Electronics, 1998, 34(4): 691–699
9. Chen W, Liu S. PIN avalanche photodiodes model for circuit simulation. IEEE Journal of Quantum Electronics, 1998, 32(12): 2105–2111
10. El-Batawy Y M, Deen M J. Modeling and optimization of resonant cavity enhanced-separated absorption graded charge multiplication-avalanche photodetector (RCE-SAGCM-APD). IEEE Transactions on Electron Devices, 2003, 50(3): 790–801
11. El-Batawy Y M, Deen M J. Analysis and circuit modeling of waveguide-separated absorption charge multiplication-avalanche photodetector (WG-SACM-APD). IEEE Transactions on Electron Devices, 2005, 52(3): 335–344
12. Banoushi A, Kardan M R, Naeini M A. A circuit model for separate absorption, grading, charge, and multiplication avalanche photodiodes. Solid-State Electronics, 2005, 49(6): 871–877
13. Mai Y X, Wang G. Equivalent circuit modeling of separate absorption grading charge multiplication avalanche photodiode. Journal of Lightwave Technology, 2009, 27(9): 1197–1202
14. Wang G, Wu J. A novel equivalent circuit model for separate absorption grading charge multiplication avalanche photodiode (APD)-based optical receiver. Journal of Lightwave Technology, 2010, 28(5): 784–790
15. Zhao Y L, Mo Q Y. An equivalent circuit model for separate absorption grading charge multiplication avalanche photodiode. Journal of Physics: Conference Series, 2011, 276(1): 012107
16. Plimmer S A, Tan C H, David J P R, Grey R, Li K F, Rees G J. The effect of an electric-field gradient on avalanche noise. Applied Physics Letters, 1999, 75(19): 2963–2965
17. Saleh M A, Hayat M M, Sotirelis P P, Holmes A L, Campbell J C, Saleh B E A, Teich M C. Impact-ionization and noise characteristics of thin III–V avalanche photodiodes. IEEE Transactions on Electron Devices, 2001, 48(12): 2722–2731
18. Goh Y L, Massey D J, Marshall A R J, Ng J S, Tan C H, Ng W K, Rees G J, Hopkinson M, David J P R, Jones S K. Avalanche multiplication in InAlAs. IEEE Transactions on Electron Devices, 2007, 54(1): 11–16
19. Masudy-Panah S, Ahmadi V. A closed form analytic model to study the characteristics of avalanche photodiodes. Journal of Modern Optics, 2009, 56(1): 67–72
20. Kim D S, Lee S Y, Lee J H, Oh G S, Kim N J, Lee J W, Kim A S, Sin Y K. Fabrication of planar InP/InGaAs avalanche photodiode without guard rings. In: Proceedings of IEEE Lasers and Electro-

Optics Society, Annual Meeting (LEOS 96). 1996, 332–333

21. Tan L J J, Ng J S, Tan C H, David J P R. Avalanche noise characteristics in submicron InP diodes. IEEE Journal of Quantum Electronics, 2008, 44(4): 378–382

22. Tarof L E, Knight D G, Fox K E, Miner C J, Puetz N, Kim H B. Planar InP/InGaAs avalanche photodetectors with a partial charge sheet in device periphery. Applied Physics Letters, 1990, 57(7): 670–672